2022 44th Annual International Conference of
the IEEE Engineering in Medicine & Biology Society (EMBC)
Scottish Event Campus, Glasgow, UK, July 11-15, 2022

2022 44th Annual International Conference of the IEEE Engineering in Medicine & Biology Society (EMBC) | 978-1-7281-2782-8/22/$31.00 ©2022 IEEE | DOI: 10.1109/EMBC48229.2022.9871754

An Immersive Virtual Reality Platform Integrating Human ECOG & sEEG: Implementation & Noise Analysis*

Courtnie J. Paschall, *Member, IEEE,* Rajesh P.N. Rao, *Senior Member, IEEE,* Jason Hauptmann, Jeffrey G. Ojemann, and Jeffrey Herron, *Member, IEEE*

***Abstract*— Virtual reality (VR) offers a robust platform for human behavioral neuroscience, granting unprecedented experimental control over every aspect of an immersive and interactive visual environment. VR experiments have already integrated non-invasive neural recording modalities such as EEG and functional MRI to explore the neural correlates of human behavior and cognition. Integration with implanted electrodes would enable significant increase in spatial and temporal resolution of recorded neural signals and the option of direct brain stimulation for neurofeedback. In this paper, we discuss the first such implementation of a VR platform with implanted electrocorticography (ECoG) and stereo-electroencephalography (sEEG) electrodes in human, in-patient subjects. Noise analyses were performed to evaluate the effect of the VR headset on neural data collected in two VR-naïve subjects, one child and one adult, including both ECOG and sEEG electrodes. Results demonstrate an increase in line noise power (57-63Hz) while wearing the VR headset that is mitigated effectively by common average referencing (CAR), and no significant change in the noise floor bandpower (125-240Hz). To our knowledge, this study represents first demonstrations of VR immersion during invasive neural recording with in-patient human subjects.**

***Clinical Relevance*— Immersive virtual reality tasks were well-tolerated and the quality of clinical neural signals preserved during VR immersion with two in-patient invasive neural recording subjects.**

I. Introduction

Modern virtual reality (VR) offers an immersive and interactive alternate world that is designed, monitored, and controlled by a VR researcher. For human cognitive and behavioral neuroscience, VR platforms grant otherwise impossible manipulation and quantification of environmental variables, including modifiable object kinematics and characteristics, the design of probability distributions to govern object interactions, adjustable world physics, and alterable "self" or avatar rendering. In addition, a virtual environment can be easily modified to accommodate the needs of individual subjects, enabling rapid iteration and customization of experimental protocols.

The flexibility and controllability of immersive VR have been exploited in animal model research for decades, though such studies often relied on animal-sized compartments to create a visual surround [1-4]. Only recently have technological advancements made immersive virtual reality accessible by headset for both human and large animal studies [5,6]. As immersive VR became more accessible, it was quickly integrated with non-invasive human neural recording modalities such as electroencephalography (EEG) and functional MRI (fMRI) to explore the neural correlates of human behavior and non-invasive brain computer interface (BCI) [5,7-9].

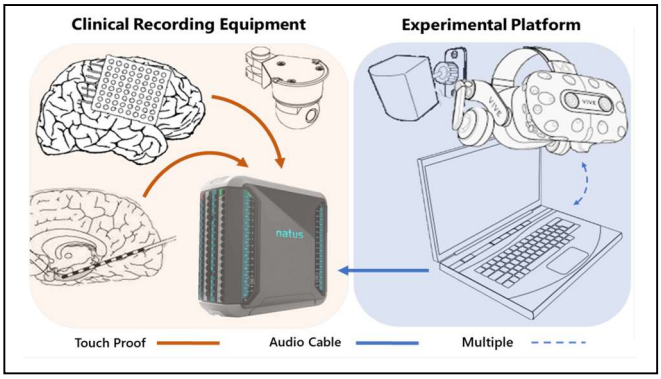

Figure 1. System diagram. (left) Clinical recording hardware includes implanted electrodes, Natus Quantum clinical neural recording suite, and in-room cameras recording continuous video and audio data. (right) The experimental VR platform includes a VR-ready gaming laptop, HTC Vive Pro Eye headset, Vive controllers 2.0, and SteamVR base stations 2.0.

Implanted intracranial electrodes offer improved spatial and temporal signal resolution over non-invasive methods by recording neural activity as voltage potentials directly from cortical and subcortical brain structures. Intracranial electrodes can also deliver direct electrical stimulation (DES) to neural tissue, which may be used as neurofeedback during behavioral tasks or in the development of bidirectional BCIs [10,11]. Recently, chronic neural implants such as deep brain stimulators (DBS) and the RNS® System (NeuroPace, Inc., Mountain View) have enabled out-patient integration of intracranial neural signals and commercial VR hardware [12].

In-patient invasive neural recording offers even greater access to human neural data through high-count electrocorticography (ECoG) and stereo-

*Research supported by the National Science Foundation (EEC-1028725) and the UW Reality Lab (sponsored by Facebook, Google, Futurewei, and Amazon). Content does not represent the official views of funding agencies.

C. J. Paschall is with the Bioengineering Department, University of Washington, Seattle, WA 98195 USA (e-mail: copa2894@uw.edu).

R. P. N. Rao is with the Paul G. Allen School for Computer Science & Engineering, University of Washington, Seattle, WA 98915 (e-mail: rpnr@uw.edu).

J. Hauptmann is with Seattle Children's Hospital, Seattle Wa 98195 (e-mail: hauptmann@seattlechildrens.org).

J. G. Ojemann & J. Herron are with the Department of Neurological Surgery, University of Washington, Seattle WA 98195 (emails: jojemann@uw.edu, jeffherr@uw.edu).

All authors are also with the Center for Neurotechnology, University of Washington, Seattle WA 98195.

electroencephalography (sEEG) electrodes that are implanted in children and adults for clinical evaluation of epilepsy. This in-patient clinical setting, however, also presents unique challenges that have traditionally precluded VR integration. Overcoming these challenges to combine the advantages of both intracranial in-patient neural recording and VR task design is an important next step for human neuroscience research.

In this work, we present a first demonstration and critical assessment of a VR task platform in human patients with invasive electrode recordings from both ECOG and sEEG. We detail our hardware setup, outline our procedure for safely and comfortably donning and removing the VR headset in this in-clinic and recently post-operative patient population, and discuss our approach to virtual immersion with VR-naïve subjects. We also characterize the impact a worn VR headset on signal noise by comparing recorded neural data acquired from two subjects during VR tasks and non-directed activities with the headset off. Our goal is to facilitate further development of immersive VR research tasks for human intracranial neural recording subjects.

II. Materials & Methods

A. Clinical Recording System & Electrode Localization

Clinical data were recorded under an approved Institutional Review Board (IRB) protocol following formal consent of the subject and their legal guardian if under 18 years of age. Data included ECOG and sEEG neural signals, in-room sound and video from wall-mounted cameras, and an audio synchronization signal used for temporal alignment of the independently recorded clinical and VR task data (See Fig. 1). Neural signals were recorded by the Natus Quantum biosignal acquisition system (Natus Medical Incorporated, San Carlos, CA) at a sampling rate of 1024 Hz, with individual contacts referenced to a scalp needle electrode and grounded to screw electrodes physically anchoring each implanted probe and. In-room video was captured at 30fps from two orthogonal views of the patient and used clinically to record preictal, during seizure, and postictal behavior. In our research, video was used to confirm alignment between data streams and label patient behavior outside of recorded task variables.

For electrode localization, preoperative Magnetic Resonance Imaging (MRI) data were acquired on a clinical Philips 3T Achieva scanner using a standard 8 channel SENSE head coil, and postoperative computerized tomography (CT) scans were acquired on a CereTom scanner (512x512x88 matrix resulting in an in-plane resolution of .5x.5 mm / 1.25 slice thickness).The preoperative T1 MRI was co-registered with post-operative CT scans using an affine registration through Statistical Parametric Mapping (SPM) software package. Three dimensional reconstructions of the pial surface were generated using FreeSurfer. Electrode channel positions were estimated from postoperative CT and projected onto the reconstructed pial surface (ECOG) or subcortex (sEEG). A secondary registration into MNI152 1mm space [http://nist.mni.mcgill.ca/icbm-152lin/] enabled automated atlas identification of each electrode.

B. Subject Demographics & Protocols

Data from two subjects implanted with intracranial electrodes for seizure localization were collected. Subject 1 was a 16 -year-old male with a prior left temporal lobectomy, implanted with 24 left temporal ECOG and 90 left hemisphere sEEG electrodes (114 in total). Subject 1 remained in VR for over 26 minutes in one continuous session. Subject 1 is, as far as the we are aware, the first in-patient subject to don an immersive virtual reality headset while undergoing invasive neural recording. Subject 2 was a 20-year-old female implanted with 142 left hemisphere sEEG electrodes. Subject 2 spent 68 minutes in VR over two sessions (12 minutes on the first day and 56 minutes on the second). As we limited analyses to controlled task periods, only data from the first session of Subject 2 were analyzed.

Our protocol for donning the headset is as follows: First, outline the full procedure to the subject -- a little nervousness is common before first immersion. Next, extend the VR headset to its maximum fit settings and note the fit mechanisms (e.g., straps or ratchets) to the subject as this is done. Then, invite the patient to hold the headset against their face in the most comfortable position for them while a researcher positions the headset strap over the "braid" of electrode cables gathered at the back of the patient's head and onto the occipital area of the skull. Finally, guide the subject's hand to the pre-introduced fit mechanisms so they may tighten their own headset for themselves. Even highly attentive researchers will not get the fit as perfect as a subject will for themselves. Secure headsets are much more comfortable over time than loose or ill-fit ones, and patient involvement in headset donning also seems to reduce pre-immersion nervousness. To remove the headset, have the patient hold the headset firmly against their face while the fit settings are loosened, and then removes the head strap mindfully. In our experience, once the subject understands the fit of the headset, they may be able to don and remove it themselves with minimal assistance from the researchers.

The two subjects in this study reported ease and comfort with donning, doffing, and wearing the headset for extended periods of time − collectively, for over an hour. In fact, both subjects opted to remain in VR when given the choice to either explore additional VR experiences (e.g., Google Earth) or remove the headset. Subject 1 spent time exploring a SteamVR mountaintop lodge scene, and Subject 2 toured Paris, Tokyo, and Volcanos National Park, HI by Google Earth VR. It may also be worth noting that while neither subject had prior experience with immersive VR (both were "VR naïve"), they each adapted to the VR tasks readily and reported neither discomfort nor symptoms of virtual reality sickness (VRS) during their experimental sessions. We highlight this to allay concerns of VRS in well-constructed VR tasks and to suggest that prior VR experience is not a prerequisite for VR task engagement.

C. Virtual Reality Platform: Hardware & Design

Our task platform (Fig. 1) utilized a VR-ready gaming laptop (Alienware m15 R4 32GB RAM NVIDIA GeForce RTX 3070 8GB) and HTC Vive Pro Eye. With a 90Hz refresh rate and a net field of view of 110°, this headset was selected to reduce the likelihood of VRS [13]. To further reduce VRS potential, tasks were designed to have simple, neutral backdrops with infinite horizons, few moving objects, and minimal requirement for head movement. All tasks were designed using the Unity Real-Time Development Platform

The HTC Vive Pro uses two SteamVR 2.0 base stations for submillimeter 6D tracking of two controllers and one headset along 3-euclidian and 3-rotational axes. In the hospital setting, base stations were mounted on extensible tripods and positioned a few feet from the hospital bed to ensure coverage of all potential dynamic movements during VR tasks. Prior to VR immersion, patients developed familiarity with the trigger, grip, and trackpad inputs of the controllers.

D. Noise Analysis: Data Collection & Preprocessing

Concurrent in-room clinical video was used to define epochs of time during which the headset was on, off, being donned, or being removed. In Subject 1, 22 continuous minutes of neural recording during which the headset was on were identified (HMD On), as well as 22 minutes with the headset off (HMD Off). On day 1 in Subject 2, epochs of 4.75 minutes and 7.23 minutes HMD On were separated by 23 minutes of neural recording HMD Off. From the intervening 23 minutes, duration-matched headset-off epochs were identified for use in subsequent analysis. In Subject 2, the neural signals recorded during headset placement enabled visualization of the headset donning and removal process on clinical recording. These data were not available in Subject 1.

Neural signals data were minimally preprocessed to preserve recorded noise. In Subject 1, four of 114 total channels were removed from subsequent analysis due to excessive volatility. This is a standard preprocessing step as such electrodes are unlikely to be recording neural signals (e.g., may not be fully implanted in neural tissue or may have a broken connection wire [14]). Two were removed due to repeated amplitude variations in excess of 4 standard deviations in both HMD On and Off conditions, and one was removed for line noise (57-62Hz) bandpower in excess of 4 standard deviations compared to other channels in HMD On and HMD Off. The fourth channel was removed due to broadband noise floor bandpower (125-240Hz) in excess of 6 standard deviations compared to other channels, but in HMD On only. Visual inspection of this channel's signal showed it to be quite noisy in both HMD On and Off conditions, though noise power increased markedly in HMD On. Noise levels decreased after headset removal, confirming the recording channel was not damaged during headset placement. This uniquely affected channel was a cortical ECoG electrode localized to the left frontal pole and was removed from the noise analysis as an outlier. In Subject 2, data from all electrodes were kept for analysis, as all sEEG channels demonstrated both similar amplitude variances and noise floor bandpower variances in HMD On and HMD Off.

Unprocessed or "raw" neural signals are local field potential (LFP) recordings natively referenced to a scalp needle electrode and grounded to a skull screw. For common average referencing (CAR), channels within each patient were referenced to the mean signal of all electrodes of a similar type. In Subject 1, all subcortical sEEG channels underwent CAR independently of ECOG channels, which were rereferenced to their own average. This independence was necessary as ECOG and sEEG electrodes have different impedance profiles. In our data, cortical ECOG channels had an average of 2.41 times the line noise power of sEEG channels in HMD On and 1.54 times in HMD Off. These ECOG vs. sEEG ratios did not change much with independent rereferencing (2.99 and 1.61, respectively) but shifted noticeably after non-independent rereferencing (0.01 and 0.02). This suggests that improper CAR may redistribute the noise in ECOG signals onto sEEG signals.

E. Noise Analysis: Noise Ratio

To help interpret the effect of noise in HMD On and Off, with and without CAR, bandpower ratios were calculated between the different recording conditions (On vs. Off) and preprocessing steps (raw vs. CAR) for each electrode. The noise ratio metric was calculated as the average of the power in the HMD On vs. Off conditions for each frequency:

$$Noise\ Ratio = \frac{1}{n}\sum_{i=1}^{n}\left(\frac{P_{on,i}}{P_{off,i}}\right),\ Power \sim \frac{V^2}{Hz} \qquad (1)$$

F. Noise Analysis: Welch's Method Power Spectral Density

To evaluate the spectral effects in HMD On neural signals, Welch method power spectral density (PSD) estimates were calculated in 1Hz frequency steps from 2 to 240Hz (1 second Hamming windows, 50% overlap, see Fig. 2). The line noise peak spanned 57-63 Hz on the PSDs, setting the frequency range for line noise analysis. In addition, a qualitative change in high frequency power was visible in HMD On vs. Off in the raw signal PSD of each patient, so a separate "noise floor" analysis was completed to quantify the power changes in this broad high frequency band (125 -240Hz). In both line noise (57-63Hz) and noise floor (125-240Hz) bands, total bandpower was calculated using an area-under-the-curve estimate by rectangular method.

G. Noise Analysis: Jensen-Shannon Divergence Metric

To evaluate the significance of bandpower changes between HMD On and HMD Off conditions, the distributions of bandpower across all electrodes were compared. The noise distributions were determined to be non-normal by chi-squared goodness of fit and Anderson-Darling tests. In response, a Jensen-Shannon Divergence (JSD) metric was used to evaluate the difference in line noise and noise floor spectral power PDFs in HMD On and HMD Off, for both raw and CAR preprocessed data. The JSD metric quantifies the distance between two probability distribution functions (PDFs), does not assume normality, and is sensitive to both translations between PDFs (e.g. a shift in noise power at all electrodes) and differences in shape (e.g. noise power changes at only a subset of electrodes).

In each frequency band, the probability distribution of bandpower values across all electrodes was fit using a kernel method. While multiple standard PDF fit functions were evaluated, the nonparametric kernel method yielded the best goodness of fit for all conditions, as assessed by a chi-squared goodness of fit (g) test calculated between the actual data's pdf and a given parametric estimate of the distribution. For Subject 1 in HMD On, for example, only the nonparametric kernel estimate yielded a statistically significant goodness of fit ($p=0.9553$, $g = 0.6672$), though other parametric fits demonstrated moderately good fit, including exponential ($p = 0.0017$), Pareto ($p=0.0033$), Log-Normal ($p=0.022$), Birnbaum-Saunders ($p=0.0310$), and Inverse Gaussian ($p=0.06$) parametric distributions. Following kernel method

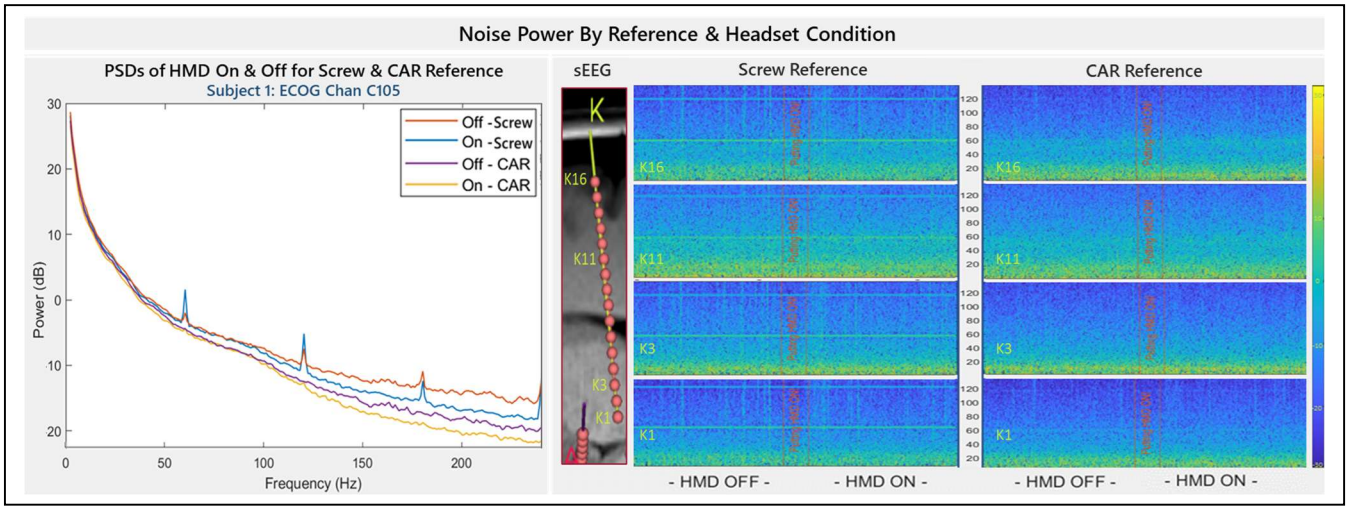

Figure 2. (left) Welch power spectral density plots of screw referenced (raw) and CAR signals in the HMD On and HMD Off conditions for an ECOG electrode (C105) in Subject 1. Note the successful removal of in-phase line noise with simple common-average rereferencing. (right) Reconstruction of an in situ sEEG electrode and stacked spectrograms for four electrodes along the probe, representing decreasing electrode label and increasing implant depth. Specifically, spectrograms of contacts 16, 11, 3, & 1, from top to bottom, are depicted. The left column depicts the screw referenced data and the right column, CAR data. Each spectrogram visualizes continuous neural signals recorded during headset donning: from HMD Off, through headset positioning (delineated by vertical red lines), to HMD On. Spectrograms demonstrate noise reduction by CAR and no significant signal perturbation during headset positioning.

fit, the JSD distance metric was calculated between HMD On and Off, in both raw and CAR preprocessed data.

To determine the statistical significance of the resultant JSD values, null distributions of JSD metrics were calculated using two distinct randomization schemes. In one, HMD On and Off labels were randomly shuffled one thousand times to create 1000 unique sets of "null" HMD On and Off distributions of spectral power values. The JSD metrics of these shuffled distributions were then calculated to create the null distribution of JSD values. This null distribution was designed to capture the range of JSD values under the null assumption that the headset condition (HMD On or Off) did not affect noise power overall, across electrodes. In the second randomization approach, 100 random power values from each of the HMD On and Off bandpower estimates were compared, bootstrapping a JSD metric to give context to the overall JSD. Though the subsamples were compared asynchronously, this randomization scheme was devised to express the range of potential JSD values within each condition's recorded data, analogous to a "confidence interval" for a given JSD comparison.

H. Exploratory Analysis: Noise Regression

Scatter plots of line noise bandpower and noise ratio vs. electrode number as an ordinal label were also drafted to visualize potential trends in the bandpower (see Fig. 3). In intracranial implants, channel 1 is the furthest from the wire bundle leaving the skull, making electrode number a rough proxy for depth from cortex, with the higher numerical labels corresponding to electrodes nearer the cortex and lower numerical labels corresponding to electrodes at greater depths. In Subject 1, all cortical ECoG electrodes were recoded to have a label of 17, which is one greater than the largest sEEG label of 16. Visible trends of the ratio of noise bandpower by contact number were then explored using a linear regression. The noise ratio metric was used to evaluate noise from the headset proportional to baseline (HMD Off) noise. To measure the effect size of a calculated regression coefficient, the Δr^2 value between it and a null regression coefficient was calculated. This null regression coefficient ($\hat{r}_{null}$) was defined as the average r_{null} of 1000 regressions with shuffled label permutations.

I. Exploratory Analysis: Headset Positioning Noise

In a final exploration, continuous neural recordings during headset positioning (donning and doffing) were identified in Subject 2 and time-frequency spectrograms built by the modified Welch method (80% overlap, reassigned center frequencies,1 sec time resolution, 2-140Hz). The spectrograms were used to visualize spectral effects during headset positioning.

III. Results

A. Noise Analysis

CAR demonstrates robust line noise removal (60Hz and calculated harmonics) in HMD On and Off in both subjects. Fig. 2 left visualizes the power spectra of HMD On and Off, raw and CAR signals, in an example cortical electrode (channel 105) from Subject 1. This figure also highlights the noise floor reduction in HMD On versus Off for both raw and CAR signals, unique to Subject 1.

Table 1 lists the mean power estimates of line noise (57-62 Hz) and high-frequency broadband noise (125-240Hz) in HMD On and Off, both before and after CAR, for both subjects. Also listed are the noise ratios comparing HMD On and Off by frequency band and reference type. These results demonstrate that CAR can efficiently remove the noise introduced by the headset: for Subject 1, the line noise ratio (on/off) was 1.266 in the raw data, indicating more line noise in HMD On. This ratio reduced to 1.017 following CAR. The noise floor ratio of 0.583 in Subject 1, raw signal, indicates a reduction in noise floor bandpower in HMD On. This ratio increased to 0.871 after CAR.

For Subject 2, results are presented for each of the epochs of matched HMD On and Off data. Again, CAR is shown to greatly reduce the noise magnitude in line and noise floor frequency bands.

TABLE I. RESULTS BY METRIC (ROW), SUBJECT & BAND (COLUMN)

	Subject 1		Subject 2 Set 1 Set 2	
	57–62 Hz	***125–240 Hz***	***57–62 Hz***	***125–240 Hz***
Noise Off (CAR) [a]	0.25 (0.15)	0.03 (0.01)	1.85 (0.27) 1.50 (0.26)	0.02 (0.01) 0.03 (0.01)
Ratio On/Off (CAR) [a]	1.27 (1.02)	0.58 (0.87)	1.01 (0.95) 0.99 (1.13)	0.56 (1.71) 1.06 (1.32)
JSD sEEG ECOG	4.48 (0.43) 2.93 (0.35) 1.55 (0.08)	14.44 (0.87) 11.65 (0.50) 2.79 (0.36)	28.62 (0.92) 2.55 (2.87)	156.20 (8.96) 4.66 (3.63)
Shuffled Range [b]	19.22 - 23.99	21.373 - 22.501	409.55 - 512.52 372.10 - 456.94	119.19 - 125.01 54.51 - 57.25
Bootstrap Range [b]	1.50 - 4.39	13.694 - 14.671	29.146 - 71.386 25.686 - 60.484	0.830 - 1.468 0.126 - 0.684
Regressions[c] ON (CAR) OFF (CAR) RATIO (CAR)	**0.08** (***0.04***) ***0.06*** (0.04) 0.002 (0.002)	**0.08** (**0.06**) **0.80** (**0.06**) **0.01** (0.002)	-0.07 (-0.21) -0.01 (-0.04) ***0.002*** (0.005) 0.009 (0.05) 0.09 (-0.04)	-0.05 (0.03) -0.03 (0.01) 0.01 (0.002) 0.02 (0.07) -0.04 (0.02)

a. Bandpower (dB) and noise ratio averaged across electrodes
b. Shuffled range approximates null distribution & Bootstrap range is akin to confidence interval
c. Correlation r with statistical significance encoded: **p<0.001**, ***p<0.01***, & not significant p>0.01

Table 1 also lists the results of the JSD analysis. Smaller JSD values indicate similarity between two distributions. The results here show much smaller JSD values between the On and Off conditions for the CAR than raw data, with JSD values much less than the range of values generated by the comparison of 1000 distributions using shuffled labels. This means that the actual On-Off distributions are more similar than 1000 random distributions generated from the data and suggests a low impact of the headset on either line noise or noise floor bandpower.

For example, in Subject 1, the JSD metric for line noise bandpower in HMD On and Off was found to be 4.482 for screw-referenced and 0.432 for CAR signal (Row 4 'JSD' in Table 1, Column 1). In 1000 randomized shuffles of on-off labels, the range of the resultant JSDs was 19.22 – 23.99 (Subject 1, line noise, raw), and in 1000 bootstrapped comparisons, the range was 1.5040 - 4.3845. For the shuffled randomization result, the real JSD was much less than the null distribution range (4.4820 < [19.22 23.99]), suggesting that the real On and Off distributions were much closer than the distances between 1000 random distributions generated from the on-off bandpower data. The bootstrapped randomization statistic (4.4820 > [1.5040 4.3845]) indicates that the calculated JSD is consistent across our data, supporting the use of the JSD metric to characterize the magnitude of difference in noise bandpower between HMD On and Off conditions.

B. Exploratory Analysis

Regressions were completed for HMD On and Off, raw and CAR, in line noise and noise floor bandpower values against electrode label. This was done to explore the relationship between VR headset noise and electrode depth. The last row of Table 1 lists abridged results for this regression analysis and Fig. 3 visualizes the results of line noise bandpower regressions for Subject 1.

For Subject 1, line noise bandpower significantly correlated with depth in both HMD On and Off, for both sEEG and ECOG electrodes. The strength of the correlation is larger in HMD On (Table 1, last row & Fig. 3, red and blue lines), indicating an increased noise gradient due to the HMD. Preprocessing with CAR reduces but does not eliminate the correlations in HMD On and Off, so while CAR may reduce both line noise magnitude and line noise gradient, it does not completely redistribute the increased line noise in the more surface sEEG electrodes and ECOG. While the regressions may be statistically significant, their Δr^2 are very small ($\Delta r^2_{\text{on-null}}$ =0.0055, $\Delta r^2_{\text{off-null}}$ =0.0027, Δr^2_{CAR} =0.0016). The noise ratio regressions for line noise bandpower conclude no significant correlation between HMD On and Off conditions for neither CAR nor raw signal.

High-frequency noise floor bandpower was shown to correlate significantly with electrode depth in HMD On and Off, both before and after CAR (Table 1). Again, the Δr^2 are quite small ($\Delta r^2_{\text{on-null}}$ =0.0055, $\Delta r^2_{\text{off-null}}$ =0.0027, Δr^2_{CAR} =0.0016). The correlation is much stronger in the off

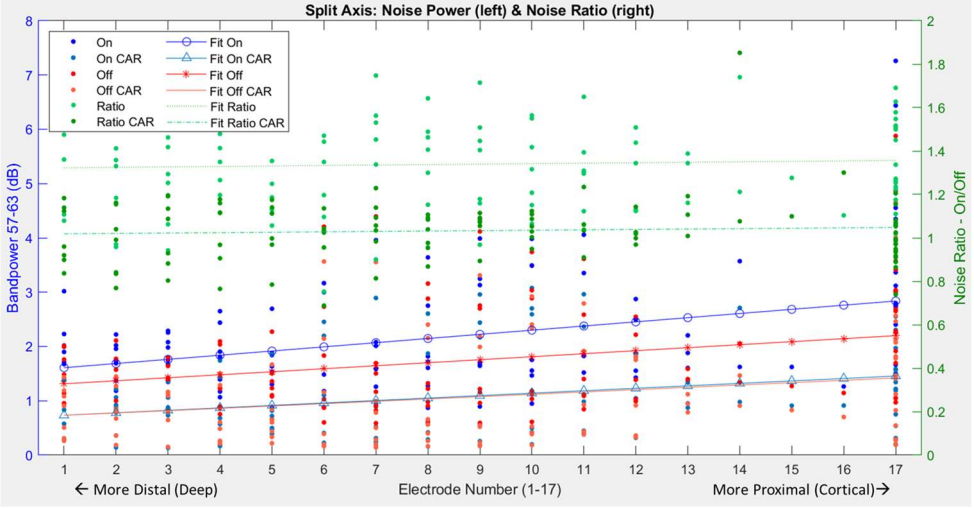

Figure 3. Line noise bandpower and regression results. Left y-axis depicts line noise bandpower (57-63Hz) for HMD On (blue & muted blue) and HMD Off (red & muted red). Right y-axis depicts noise ratio (green & muted green). The shared x-axis encodes electrode labels from 1-17, with 1 deepest to 16 shallowest/most cortical sEEG, and ECOG recoded as 17. The scatterplots show data distribution per condition. For Subject 1, a significant noise correlation with electrode label for HMD On (blue) and Off (red) is seen, with a steeper regression slope in HMD On. CAR reduces HMD On and Off (muted red & muted blue) noise power and flattens the HMD On gradient. (left axis) Raw noise ratio data show a nearly flat regression and are reduced towards 1 by CAR.

condition, which agrees with the earlier result that the headset reduced the overall noise floor in Subject 1. This result suggests it does so by reducing high-frequency noise in the most cortical electrodes, seen as a reduced gradient (regression slope) in HMD On vs. HMD Off. The significant correlation of noise floor ratio and electrode label seen in the raw data does not survive CAR, suggesting that CAR redistributes high-frequency broad band noise.

In Subject 2 (sEEG only), bandpower did not significantly correlate with depth in any condition or frequency band. While the ratio of headset bandpower correlated with electrode label in both raw and CAR data for set 2, the effect sizes were very small ($\Delta r^2_{\text{ratio-null}}$ =0.00004, $\Delta r^2_{\text{ratioCAR-null}}$ =0.00080). Ratio correlations were not significant in the noise floor frequency band.

Stacked spectrograms were used to visualize continuous resting state spectral data during HMD Off, headset positioning, and HMD On (Fig. 2). Each spectrogram represents the same epoch of time, during which Subject 1 was at rest and not wearing the VR headset, then donning the headset with assistance, and then sitting in a virtual "waiting room" depiction of a dark sky at dusk. The spectrograms demonstrate the effectiveness of CAR in reducing line noise in both On and Off conditions. They also confirm that headset donning procedure does evoke significant changes or artifacts in the spectral time series. Signal stability was present during all epochs of headset manipulation.

IV. Discussion

Virtual reality behavioral task design represents a new and emerging platform for human neuroscientific research. In this work, we discussed a first implementation of a VR experimental platform with in-patient subjects undergoing invasive neural monitoring for seizure localization. We also quantified the impact of the VR system on electrophysiological signal quality in intracranial recordings.

In our noise analysis, we explored the impact of electrical noise from the VR headset, demonstrating efficient removal of headset-induced line noise (57-63Hz) using simple CAR preprocessing. In Subject 1, an exploratory regression analysis revealed a significant relationship between line noise bandpower and electrode label, a proxy of electrode depth, in HMD On and Off. This indicates an increased susceptibility to line noise in the shallower or more cortical electrodes, the ones most proximal to the site of surgical implantation. The regression remained significant following CAR, although the magnitude of the line noise and the $\Delta r2$ (effect size) of the regression were reduced. Collectively, these results suggest that while the headset increases line noise in neural recordings, this increase is readily addressed by a simple CAR preprocessing step. The headset was also seen to either decrease or minimally impact the broadband high frequency noise floor (125-240Hz), preserving this important and often low signal-to-noise spectral region.

In this paper, we also discussed successful approaches and considerations for VR immersion in an in-clinic, invasive neuromonitoring patient population, and outlined VR hardware selection, basic room setup, and patient interaction protocols. We also sought to address concerns about VR skill acquisition in VR-naïve populations, noting the rapid VR immersion, task engagement, and genuine enthusiasm from both patients for our VR tasks. Although a small sample size, our first two subjects not only tolerated their VR experiences but were eager to remain in VR. Neither subject, at any point, expressed discomfort with VR immersion or demonstrated signs of VRS.

This work represents, to the best of our knowledge, the first implementation of an immersive VR task for patients implanted with intracranial electrodes in an in-patient setting. The analysis and discussion are intended to facilitate adoption of VR platforms in this patient population.

Acknowledgment

We would like to thank Dr. Alexander Doud for clinical data retrieval. We also gratefully acknowledge the incredible patients who participate in this research.

References

[1] H. J. Dahmen, "A simple apparatus to investigate the orientation of walking insects," *Experientia*, vol. 36, no. 6, pp. 685–687, Jun. 1980.

[2] C. Hölscher, A. Schnee, H. Dahmen, L. Setia, and H. A. Mallot, "Rats are able to navigate in virtual environments," *J. Exp. Biol.*, vol. 208, no. Pt 3, pp. 561–569, Feb. 2005.

[3] M. Minderer, C. D. Harvey, F. Donato, and E. I. Moser, "Neuroscience: Virtual reality explored," *Nature*, vol. 533, no. 7603, pp. 324–325, May 2016.

[4] J. R. Stowers *et al.*, "Virtual reality for freely moving animals," *Nat. Methods*, vol. 14, no. 10, pp. 995–1002, Oct. 2017.

[5] C. J. Bohil, B. Alicea, and F. A. Biocca, "Virtual reality in neuroscience research and therapy," *Nat. Rev. Neurosci.*, vol. 12, no. 12, pp. 752–762, Nov. 2011.

[6] D. Castelvecchi, "Low-cost headsets boost virtual reality's lab appeal," *Nature*, vol. 533, no. 7602, pp. 153–154, May 2016.

[7] J.-P. Tauscher, F. W. Schottky, S. Grogorick, P. M. Bittner, M. Mustafa, and M. Magnor, "Immersive EEG: Evaluating Electroencephalography in Virtual Reality," in *2019 IEEE Conference on Virtual Reality and 3D User Interfaces (VR)*, Mar. 2019, pp. 1794–1800.

[8] S. G. Mason, A. Bashashati, M. Fatourechi, K. F. Navarro, and G. E. Birch, "A comprehensive survey of brain interface technology designs," *Ann. Biomed. Eng.*, vol. 35, no. 2, pp. 137–169, Feb. 2007.

[9] D. Camargo-Vargas, M. Callejas-Cuervo, and S. Mazzoleni, "Brain-Computer Interfaces Systems for Upper and Lower Limb Rehabilitation: A Systematic Review," *Sensors* , vol. 21, no. 13, Jun. 2021, doi: 10.3390/s21134312.

[10] J. A. Cronin *et al.*, "Task-Specific Somatosensory Feedback via Cortical Stimulation in Humans," *IEEE Trans. Haptics*, vol. 9, no. 4, pp. 515–522, Oct. 2016.

[11] D. J. Caldwell, J. G. Ojemann, and R. P. N. Rao, "Direct Electrical Stimulation in Electrocorticographic Brain-Computer Interfaces: Enabling Technologies for Input to Cortex," *Front. Neurosci.*, vol. 13, p. 804, Aug. 2019.

[12] U. Topalovic et al., "Wireless Programmable Recording and Stimulation of Deep Brain Activity in Freely Moving Humans," Neuron, vol. 108, no. 2, pp. 322–334.e9, Oct. 2020.

[13] P. Kourtesis, S. Collina, L. A. A. Doumas, and S. E. MacPherson, "Technological Competence Is a Pre-condition for Effective Implementation of Virtual Reality Head Mounted Displays in Human Neuroscience: A Technological Review and Meta-Analysis," *Front. Hum. Neurosci.*, vol. 13, p. 342, Oct. 2019.

[14] G. Li *et al.*, "Optimal referencing for stereo-electroencephalographic (SEEG) recordings," *Neuroimage*, vol. 183, pp. 327–335, Dec. 2018.